



Evaluating the Potential of Rhyolitic Glass as a Lithium Source for Brine Deposits

B. S. Ellis,^{1,†} D. Szymanowski,² C. Harris,³ P.M.E. Tollan,¹ J. Neukampf,^{1,4} M. Guillong,¹
E. A. Cortes-Calderon,¹ and O. Bachmann¹

¹*Institute of Geochemistry and Petrology, ETH Zurich, 8092 Zurich, Switzerland*

²*Department of Geosciences, Princeton University, Princeton, New Jersey 08544, USA*

³*Department of Geological Sciences, University of Cape Town, 13 University Avenue, Rondebosch 7701, South Africa*

⁴*CNRS, Centre de Recherches Pétrographiques et Géochimiques, 15 rue Notre Dame des Pauvres BP 20,
F-54500 Vandœuvre les Nancy, France*

Abstract

Lithium is an economically important element that is increasingly extracted from brines accumulated in continental basins. While a number of studies have identified silicic magmatic rocks as the ultimate source of dissolved brine lithium, the processes by which Li is mobilized remain poorly constrained. Here we focus on the potential of low-temperature, post-eruptive processes to remove Li from volcanic glass and generate Li-rich fluids. The rhyolitic glasses in this study (from the Yellowstone-Snake River Plain volcanic province in western North America) have interacted with meteoric water after emplacement as revealed by textures and a variety of geochemical and isotopic signatures. Indices of glass hydration correlate with Li concentrations, suggesting Li is lost to the water during the water-rock interaction. We estimate the original Li content upon deposition and the magnitude of Li depletion both by direct in situ glass measurements and by applying a partition-coefficient approach to plagioclase Li contents. Across our whole sample set (19 eruptive units spanning ca. 10 m.y.), Li losses average 8.9 ppm, with a maximum loss of 37.5 ppm. This allows estimation of the dense rock equivalent of silicic volcanic lithologies required to potentially source a brine deposit. Our data indicate that surficial processes occurring post-eruption may provide sufficient Li to form economic deposits. We found no relationship between deposit age and Li loss, i.e., hydration does not appear to be an ongoing process. Rather, it occurs primarily while the deposit is cooling shortly after eruption, with $\delta^{18}\text{O}$ and δD in our case study suggesting a temperature window of 40° to 70°C.

Introduction

Lithium is an economically important element, particularly for glass manufacturing, synthesis of lubricating greases, and rechargeable Li-based batteries (Bibienne et al., 2020). Economic deposits of Li are found predominantly as pegmatites (London and Morgan, 2017), brine deposits (Munk et al., 2016), and sediment-hosted clay deposits (e.g., Castor and Henry, 2020). While hard rock (i.e., pegmatite) sources are currently the most exploited (Bowell et al., 2020), it is estimated that 70% of global Li reserves lie in brine deposits (Sterba et al., 2019). The major brine deposits are primarily found in moisture-limited, closed continental basins, for example, in South America (the “Lithium Triangle” of Chile, Argentina, and Bolivia) and China (Kesler et al., 2012), that act as focal points for water-soluble Li derived from various sources in the drainage area. The current model for the formation of Li brine deposits requires a number of independent factors to come together. The most important of these are a suitably arid climate, a closed hydrologic system, related igneous or geothermal activity, tectonic subsidence of the region, appropriate source rocks, and sufficient time for numerous superimposed processes to act to concentrate the brine (Bradley et al., 2013; Munk et al., 2016).

As Munk et al. (2016) point out, along with the timescale, the source rock factor (of the six critical factors listed above) remains the least well understood. A number of previous studies have speculated that surficial weathering of rocks, particularly volcanic rocks, or inputs from geothermal fluids may play

a significant role in delivering Li to brine deposits (e.g., Lowenstein and Risacher, 2009; Kesler et al., 2012; Godfrey et al., 2013; Hofstra et al., 2013; Munk et al., 2016). From literature compilations in Tomascak et al. (2016), it can be observed that many potential crustal lithologies (granites, metamorphic rocks, sedimentary rocks) have Li contents in the tens of ppm and sometimes exceeding 100 ppm. Among those, volcanic rocks have been widely implicated (Kesler et al., 2012; Hofstra et al., 2013; Benson et al., 2017a; Munk et al., 2018) as a likely source of Li for brine deposits for two primary reasons. The first is the observation that such lithologies appear to have a spatiotemporal association with the known brine deposits. Second, because it is moderately incompatible in most major magmatic phenocryst phases, Li is enriched by fractional crystallization such that the most evolved magmas (i.e., rhyolites) typically contain an order of magnitude more Li than the well-established ~4 to 13 ppm found in mid-ocean ridge basalt (MORB) (Tomascak et al., 2016; Chen et al., 2020). Based on the compilation of Chen et al. (2020) with additional data from Swallow et al. (2019), silicic volcanic rocks (taken here as those with $\text{SiO}_2 > 68$ wt %) have bulk Li contents of 0 to 240 ppm (App. 1, Fig. A1). The Li contents appear independent of the tectonomagmatic setting with average Li concentrations from global volcanic arcs (30.8 ± 28.5 , $n = 358$), volcanic rocks from the Andes (40.6 ± 38.4 , $n = 89$), and from the Yellowstone province (32.5 ± 14.5 , $n = 95$) broadly overlapping (App. 1, Fig. A1). While use of bulk rock data to describe the behavior of potentially volatile elements comes laden with complications, a first-order observation is that rocks from the Andes (that host economic brine deposits) are not necessarily signifi-

[†]Corresponding author: e-mail, ben.ellis@erdw.ethz.ch

cantly enriched in Li compared with those from Yellowstone (that do not). This emphasizes the first-order role for hydrologic processing in forming brine deposits and suggests that given the compositional similarity between the two regions, understanding how Li is liberated from volcanic deposits in either region is likely to be informative for the process as a whole. Overall, evolved magmatic rocks (broadly rhyolites) likely represent the largest repository for Li in brine source areas both volumetrically and in terms of abundance.

The Li content of rhyolitic magmas prior to eruption is a subject of much debate. Studies of quartz-hosted melt inclusions produce an intriguing array of results. Naturally glassy inclusions from a range of tectonic settings typically have Li contents from tens to a few hundred ppm with values slightly elevated above groundmass glass values (Dunbar and Hervig, 1992; Stix and Layne, 1996; Wallace et al., 1999; Anderson et al., 2000; Myers et al., 2016). In contrast, studies that have used crystallized melt inclusions either measured directly (e.g., Neukampf et al., 2019) or rehomogenized (e.g., Hofstra et al., 2013; Benson et al., 2017a) report significantly higher values (hundreds to thousands of ppm Li), hinting at Li enrichment during or after the crystallization of the melt inclusion. Thus, original Li contents of melts remain elusive. This problem is exacerbated by the potential for Li to partition into a magmatic volatile phase (be it a liquid or a gas) prior to or during eruption and by the rapid rates of Li diffusion through vapor, melt, and crystals. A variety of studies have suggested that at shallow upper-crustal pressures, Li may preferentially partition from a melt into a vapor (Kent et al., 2007; Lowenstern et al., 2012; Neukampf et al., 2021), into a magmatic brine (Webster et al., 1989), or indeed remain in the melt phase (Iveson et al., 2019).

Given the complex and relatively underconstrained behavior of this element before, during, and shortly after an eruption, it is key to clearly distinguish between the magmatic and the postmagmatic budget of Li. Upon eruption, deposition, and cooling of a volcanic rock forming a lava or a pyroclastic deposit, the starting balance of Li in magma is distributed among the erupted melt, crystals, and any gas/brine phases released during eruption, transport, and cooling. A volcanic deposit is therefore likely to be already depleted in Li by previous pre- and syneruptive loss (Lowenstern et al., 2012; Neukampf et al., 2021). As a deposit undergoes cooling, it may experience further degassing (e.g., 25% Li loss from the interior of the rhyolitic Tuff of Knob; Ellis et al., 2018) and internal redistribution of Li driven by groundmass crystallization (Ellis et al., 2015, 2018). While surface degassing of volcanic rocks may contribute an unknown quantity of Li to the hydrologic system, the rocks themselves are most likely the main reservoir of Li for forming a Li brine deposit. Therefore, the primary focus in constraining sources to economic deposits should be on understanding the original content and distribution of Li in pristine volcanic rocks at the time of deposition, rather than in the magma that sourced them.

Among the many evolved volcanic lithologies, glassy varieties of rocks in particular have been suggested as fertile sources of Li (e.g., Hofstra et al., 2013; Benson et al., 2017a). This is primarily due to the moderately incompatible behavior of Li in most magmatic minerals (Neukampf et al., 2019), which acts to concentrate it in volcanic groundmass as a result

of magmatic differentiation. Depending on the cooling rate, this Li-rich groundmass may crystallize to form a fine-grained matrix or quench to glass. As volcanic glass is thermodynamically unstable in ambient atmospheric conditions, it is thought to be more susceptible to weathering processes and potential loss of Li than other crystalline lithologies where Li is structurally bound in minerals.

In this study, we focus on rhyolitic glass as an easily accessible source of mobile Li and consider the mechanism and magnitude of Li loss from rhyolitic volcanic deposits following emplacement in order to evaluate their potential to be ultimate sources of Li for brine deposits. We investigated this using a large set of geochemical analyses of rhyolites from the Yellowstone-Snake River Plain volcanic province (Nevada-Idaho-Wyoming, NW United States). The rhyolites of the Snake River Plain are not known to be associated with any Li brine deposits (although most of the presumptive caldera basins remain obscured by younger basalt flows); however, one of the oldest Yellowstone-Snake River Plain eruptive centers, the c. 16.4 Ma McDermitt caldera, hosts a significant sediment-hosted claystone Li deposit (Benson et al., 2017b; Henry et al., 2017; Castor and Henry, 2020). While not economic, the studied Yellowstone-Snake River Plain rhyolites do provide a temporally constrained archive of Li loss from continental volcanic rocks spanning more than 10 m.y. As such, they offer an excellent analogue for other, less well-studied settings where large volumes of evolved volcanic rocks are available to interact with surface water or groundwater, leading to Li-enriched waters and brines. To understand how Li may be liberated from volcanic glass, we combine a variety of geochemical and isotopic proxies to define the extent of hydration of the glass and use this as a framework within which to interpret Li loss.

Sample Selection

In this study, we use the large existing library of rhyolitic glass and mineral compositions from the Yellowstone-Snake River Plain volcanic province (data compiled from Ellis et al., 2015, 2017, 2018; Neukampf et al., 2019) and combine these data with new analyses (all new results presented here are found in Appendices A1–A8). The rhyolites of the Snake River Plain display an association of lithofacies that are sufficiently distinct to be classified as “Snake River-type” volcanism (Branney et al., 2008). The rhyolites in this study are characteristically “hot and dry” and contain an anhydrous phenocryst assemblage of plagioclase, sanidine, quartz, augite, pigeonite, ilmenite, and titanomagnetite with accessory zircon and apatite (e.g., Bonnichsen and Citron, 1982; Cathey and Nash, 2004). Both ignimbrites and lavas of the Yellowstone-Snake River Plain have a characteristic internal lithostratigraphy whereby typically thin glassy regions at the margins of the deposit are separated by a thick microcrystalline portion that volumetrically dominates (~90%). This lithological dichotomy is imposed on the deposits as a result of differing cooling rates following eruption. Where the cooling rates in the insulated interior of the deposit are sufficiently low, the silicate melt crystallizes with a range of textures but with a mineralogy dominated by sanidine, quartz, and plagioclase as dictated by its rhyolitic composition (e.g., Ellis et al., 2015). Our sample set contains data from both lavas and ignimbrites and spans ~10 m.y. By maintaining a focus across a

single volcanic province, we minimize the number of potential variables (e.g., the mineral assemblage, the bulk composition, the climatic influence) that can be acting to modify the removal of Li from rhyolitic glass post-eruption. In addition to this province-wide scale, we focus in detail on the glasses within a single eruptive deposit, Cougar Point Tuff XI.

Cougar Point Tuff XI

Cougar Point Tuff XI is a voluminous ignimbrite ($\geq 350 \text{ km}^3$) erupted from the Bruneau-Jarbridge eruptive center of the Yellowstone hot spot track in southern Idaho/northern Nevada at about 11.4 Ma (Ellis et al., 2012). The quickly cooled basal portion of the Cougar Point Tuff XI ignimbrite contains three distinct morphologies of volcanic glass that have undergone different post-eruptive histories (Fig. 1). Overlying a well-developed paleosol that records an eruptive hiatus prior to the Cougar Point Tuff XI eruption, a nonwelded fallout deposit of coarse ash of a few tens of centimeters thickness represents the earliest erupted material. The base of the ignimbrite above the fallout layer is a dense vitrophyre formed through rapid cooling against the substrate, with the lower portion extensively perlitized. Above the vitrophyre, where cooling rates were lower, the greater part of the deposit is characterized by a microcrystalline groundmass.

Methods

Imaging and electron microprobe analyses

Prior to geochemical analyses, glass fragments separated from glassy facies of each deposit were embedded in 1-inch epoxy mounts, polished, and carbon coated. Backscatter electron images (BSE) were obtained using a JEOL JSM-6390 scanning electron microscope (SEM) at ETH Zürich. The major and minor element composition (Si, Na, Mg, Al, Ca, Cl, K, Ti, P, Fe, Mn, Cr) of the glass was determined using a JEOL JXA 8230 Superprobe electron microprobe at ETH Zürich. Profiles were measured with a 20 to 25 μm step size with a secondary reference material measured every 40 to 60 measurements. All analyses were obtained with an acceleration voltage of 15 kV, a beam diameter of 20 μm , and a beam current of 10 nA using a counting time of 20 s on peak and 10 s background. Only chlorine was measured with 30 s on peak and 15 s background and titanium with 20 s on peak and 20 s background. All analyses were performed so that Na and K (elements mobile under the electron beam) were measured first, with NIST 610, NIST 612, and VG-568 72854 rhyolitic glass used as secondary reference materials (data provided in App. Table A7). To ensure that electron beam-induced alkali migration was not affecting our results, we reanalyzed the Cougar Point Tuff XI glasses under identical analytical conditions and reprocessed the data using a time-dependent intensity correction to monitor potential alkali loss during analysis. Such correction was performed using the Probe for EPMA software (Donovan et al., 2007). The results indicate minimal migration of sodium or potassium (App. Table A8, Fig. A2).

Laser ablation-inductively coupled plasma-mass spectrometry (LA-ICP-MS) analyses

LA-ICP-MS trace element analyses were carried out at ETH Zürich using an Australian Scientific Instruments (now Ap-

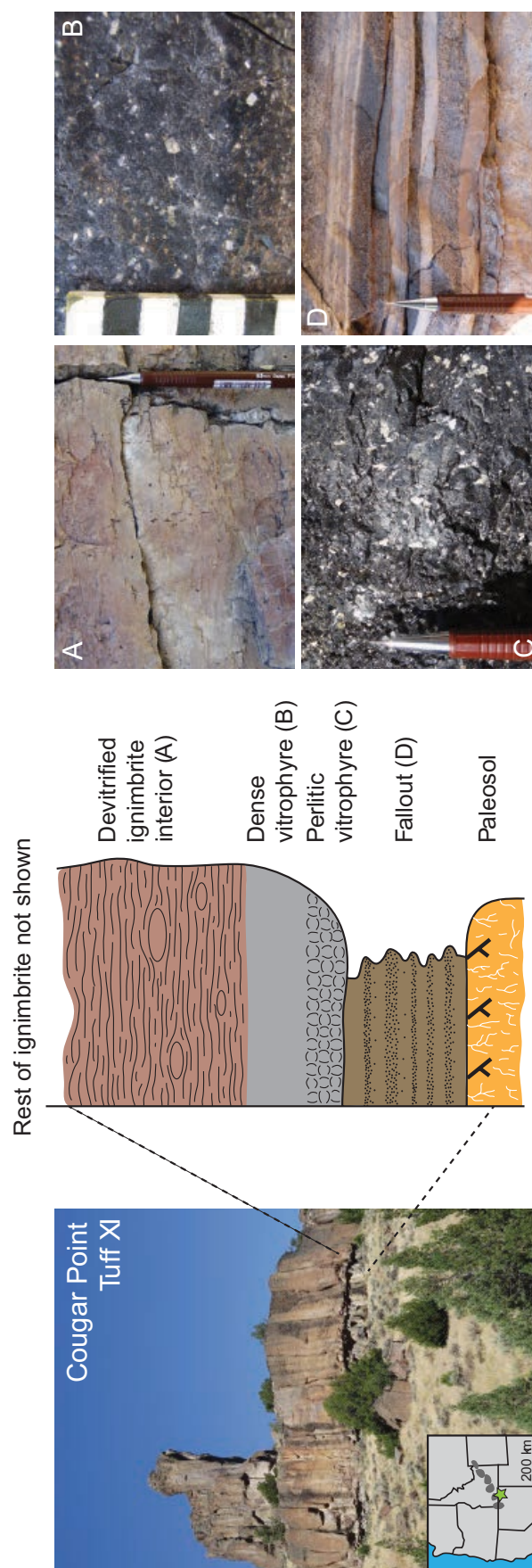


Fig. 1. Overview of the geologic setting of Cougar Point Tuff XI. Samples were collected from 41.98834°N, 115.41222°W. Scale bar in B is graduated in cm.

plied Spectra) Resolution-LR 193 nm ArF excimer laser with S155 2-volume cell, connected to a Thermo Element XR sector field ICP-MS. Ablation was conducted for 30 s at 5 Hz using mostly a 43- μm -diameter spot. Ablated material was extracted in a stream of He (500 mL/min) and then mixed with Ar (1 L/min) and N (2 mL/min) before entering the plasma. Data were reduced similarly to Szymanowski et al. (2015) using the SILLS program (Guillong et al., 2008), NIST 612 as the primary reference material, and an internal standard of SiO_2 as appropriate for each sample. Synthetic glasses GSD-1G and ATHO-G were interspersed every 25 to 30 unknowns and used as secondary reference materials. Long-term performance of the instrument (App. 1, Fig. A3) based on repeat analyses of the GSD-1G reference material over the past six years indicates that reproducibility of Li abundances is on the order of $\sim 5\%$, with a global average of 42.5 ± 2.1 ppm ($n = 343$, 2 standard deviations) in good agreement with the preferred value of 43 ± 6 ppm (GeoReM database, accessed July 2020; Jochum et al., 2005).

Oxygen and hydrogen isotopes

The O and H isotope ratios were determined on powdered aliquots coming from glass separates of between 120 mg and 1 g picked under a binocular microscope, with analyses carried out in the Department of Geological Sciences, University of Cape Town. Following drying, samples for $\delta^{18}\text{O}$ were degassed under vacuum and processed on a conventional silicate line following methods described by Vennemann and Smith (1990) and Harris et al. (2002). The internal quartz standard, Murchison Quartz (MQ) ($\delta^{18}\text{O}_{\text{SMOW}} = 10.1\text{‰}$) was run along with unknowns and used to normalize data to the standard mean ocean water (SMOW) scale. Over the course of this work, the average difference between duplicates of MQ was $\delta^{18}\text{O} = 0.21\text{‰}$ ($n = 3$). Hydrogen isotopes and water contents of the same powdered glass separates were determined using the method of Vennemann and O'Neil (1993). Briefly, raw data were normalized to SMOW (and corrected for compression) using the water standards RMW ($\delta\text{D} = -131.4\text{‰}$) and CTMP2010 ($\delta\text{D} = -7.4\text{‰}$) with the in-house Serina kaolinite analyzed with the unknowns (Serina bulk kaolinite, $\delta\text{D} = -57\text{‰}$, $\text{H}_2\text{O} = 12.4$ wt %; Harris et al., 1999). The measured δD values of the standard gave an average of $-59.5 \pm 3.6\text{‰}$ (2σ , $n = 3$) after corrections to the raw data. All data were adjusted to the accepted Serina kaolinite value. Water abundances (as H_2O^+) were measured from the voltage on the mass 2 collector of the mass spectrometer. This was calibrated against measured volumes of standard waters analyzed alongside the unknowns. The measured water content gave 12.42 wt % (± 0.5 wt % 2σ , $n = 3$). USGS57 biotite and USGS58 muscovite were analyzed with the unknowns and gave $\delta\text{D} = -94$ and -26‰ , and 2.84 and 3.95 wt % water, respectively. Accepted values are $\delta\text{D} = -91.5$ and -28.4‰ , and 3.74 and 4.03 wt % water.

Cougar Point Tuff XI Results

Glass

Morphologies: Rhyolitic glasses from the Yellowstone-Snake River Plain exhibit a wide range of morphologies depending on the eruptive dynamics and the post-eruptive history of the

material. Here, we take Cougar Point Tuff XI as an example of the variability in glass as it contains three distinct glass types: shards (forming the fallout, Fig. 1D), dense vitrophyre (Fig. 1B), and perlitic vitrophyre (Fig. 1C). The glass shards have domains of glass hundreds of microns thick separating equally large remnant vesicles. Such morphologies are quite distinct from the typical microvesicular nature of rhyolitic pumice and are characteristic of the nonwelded tephra in Snake River-type eruptions (Branney et al., 2008). Notably, these nonwelded shards are perfectly homogeneous in appearance, showing no sign of perlitic cracking or variations in backscatter brightness (Fig. 2). The perlitic vitrophyre samples are significantly more heterogeneous on a submillimeter scale. In places, these samples of perlitic vitrophyre show trains of nanometer-scale Fe-Ti oxides within the glass that trace out the margins of former glass shards that agglutinated together syn- or postdeposition during rheomorphism (e.g., Andrews and Branney, 2011). These Fe-Ti oxide traces are then cut by thin, curvilinear fractures that characterize perlitized glasses from other locations. These perlitic fractures may or may not be associated with a lightening of the grayscale backscatter intensity. The uppermost sample, that of the dense vitrophyre, contains a different suite of textures. In these samples, the trains of Fe-Ti oxides that occur in the perlitic sample have not been observed. Perlitic cracks still occur in these glasses but to a much lower extent, while the lighter zones in BSE images are more common and may occur with or without associated cracks (Fig. 2).

Major and trace element contents: Glass compositions from the three morphologies from Cougar Point Tuff XI (individual shards, perlitized vitrophyre, and dense vitrophyre; Fig. 2) are all rhyolitic, with major and trace element contents that are in good agreement with previously published compositions, allowing for differences in methodologies (Cathey and Nash, 2004). In detail, the shards (JN36) have slightly higher average SiO_2 contents (recalculated anhydrous) than the glasses from the vitrophyre (77.4 to 76.4 wt %) and have identical TiO_2 and CaO contents. The most stark difference between the glass types is the variability in their K_2O and Na_2O contents and consequently their $\text{K}_2\text{O}/\text{Na}_2\text{O}$ ratio (Fig. 3). Electron microprobe analytical totals, commonly used as a proxy for the amount of hydration of volcanic glass, the “water by difference method,” are similar between the different morphologies (shards 95.8–97.1%, avg 96.4%, $n = 39$; dense vitrophyre 95.2–98.9%, avg 96.8%, $n = 224$; perlitic vitrophyre 94.7–98.4%, avg 96.7%, $n = 318$) and in excellent agreement with previous estimates of water contents of 2.0 to 3.2 wt % based on the difference between calculated and stoichiometric oxygen (Cathey and Nash, 2004).

Lithium contents of Cougar Point Tuff XI glass range from 13.3 to 37.2 ppm. Overall, this range is similar to that previously published for rhyolitic glasses of the Snake River Plain (Ellis et al., 2018). In detail, the nonwelded glass shards that are texturally homogeneous (JN36, Fig. 2) have the highest Li contents with the least variability, while those from the other glass morphologies are somewhat lower (Fig. 4). Li is considered to be an incompatible element in rhyolitic magmatic systems (Neukampf et al., 2019), yet there is little relationship between Li and other incompatible elements (e.g., Rb), suggesting that the variability observed in Li in samples JN37 and JN40 is unlikely

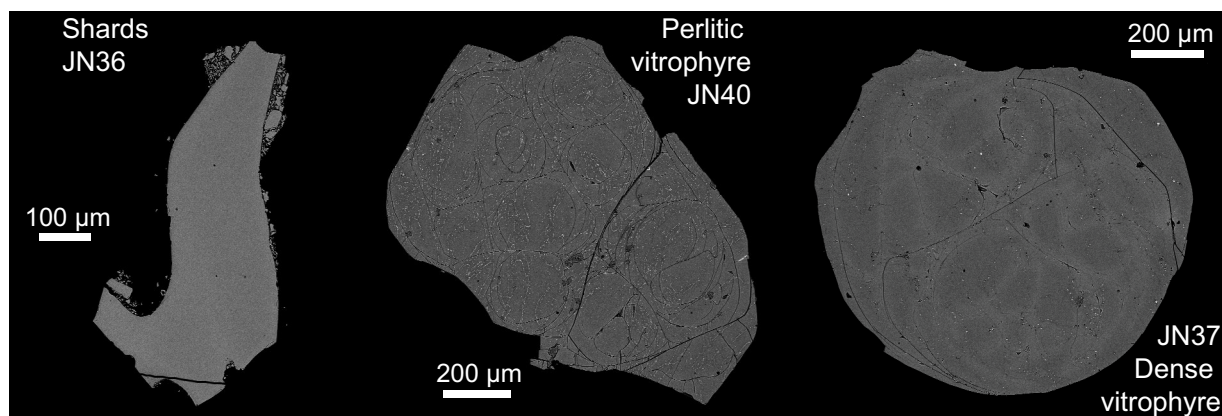


Fig. 2. Appearance of the different Cougar Point Tuff XI glass morphologies in backscattered electron (BSE) imaging. Notably, the shards from the fallout (sample JN36) contain pure glasses, while those from the ignimbrite vitrophyres show micro-lites of iron oxides and superimposed perlitic cracks.

to reflect a magmatic process. There exists, however, a strong correlation between the Li content and the K/Na ratio, a ratio that is well established to be controlled by the post-eruptive hydration of volcanic glass (e.g., Lipman et al., 1969).

Stable isotope compositions: Oxygen isotopic compositions of bulk glass separates from different size fractions of the three samples range from $\delta^{18}\text{O} = 4.8$ to 8.4‰ (Table 1). No relationship exists between either the grain size of the sample or the particular sample and the resultant $\delta^{18}\text{O}$ value. The δD values range from -155 to -133‰ with the JN37 sample having distinctly higher values (-134 to -133‰) than the other samples (-155 to -145‰). The water contents of the bulk glasses range from 0.85 to 1.62 wt % and roughly track the δD values, with higher water contents typically associated with more negative δD .

Feldspar phenocryst compositions

Plagioclase compositions from Cougar Point Tuff XI have previously been well characterized in terms of major elements as having compositions of An_{24-32} (Cathey and Nash, 2004; Ellis et al., 2012) with scant compositional zonation within a crystal. In terms of trace elements, the plagioclase crystals are typical of

Yellowstone-Snake River Plain rhyolites, with Sr and Ba contents averaging 339 ppm and 1,250 ppm, respectively. Their Li contents range from 2.2 to 7.5 ppm, with an average of 4.4 ± 0.9 ($n = 217$, 1 s). The Li content and the low variability within and between crystals is typical of plagioclase from vitrophyres of Yellowstone-Snake River Plain rhyolites in our compilation (Fig. 4, data in App. Tables A4, A5).

Discussion

Hydration of volcanic glass

It has long been recognized that volcanic glasses that interact with meteoric water postdeposition undergo hydration (Friedman and Smith, 1958; Lipman, 1965; Noble, 1967; Lipman et al., 1969; Jezek and Noble, 1978). These and other studies illustrate that post-eruptive hydration of volcanic glasses generally results in a decrease in the sodium and an increase in the potassium contents of deposits, while other elements (e.g., Al) remain unaffected. Microcrystalline lithologies are thought to be closer to the original unmodified composition upon deposition (e.g., Lipman, 1965). Taking these as the starting point, it is apparent that hydration is affecting the composition of rhyo-

Table 1. Hydrogen and Oxygen Isotope Ratios and Water Contents of Cougar Point Tuff XI Glass

Sample	Morphology	Diameter (mm) ¹	$\delta^{18}\text{O}$ (‰)	δD (‰)	H_2O (wt %)	δD meteoric water (‰) ²	$\delta^{18}\text{O}$ meteoric water (‰) ³
JN36	Shards	1–2	7.7 ⁴	–155	1.61	–140	–18.8
JN37	Dense	0.5–1	4.9	–134	1.18	–119	–16.1
JN37	Dense	1–2	7.2	–133	0.85	–118	–16.0
JN37	Dense	>2	8.4	–134	0.95	–119	–16.1
JN40A	Perlitic	0.5–1	6.9	–145	1.11	–130	–17.5
JN40A	Perlitic	1–2	6.5	–145	1.13	–130	–17.5
JN40A	Perlitic	>2	6.1	–148	0.96	–133	–17.9
JN40B	Perlitic	0.5–1	4.8	–153	1.26	–138	–18.5
JN40B	Perlitic	1–2	5.8	–153	1.26	–138	–18.5
JN40B	Perlitic	>2	4.8	–153	1.62	–138	–18.5

All isotope data relative to standard mean ocean water

¹ Size of the crushed fraction that the glass was picked from

² Estimate of meteoric water δD calculated using an approximate high-T glass-water δD per mil fractionation of -15‰ (Bindeman and Lowenstern, 2015) without correction for residual magmatic water

³ Assuming meteoric water follows the global meteoric water line ($\delta\text{D} = 8 \delta^{18}\text{O} + 10$)

⁴ Laser fluorination value, others via conventional analysis

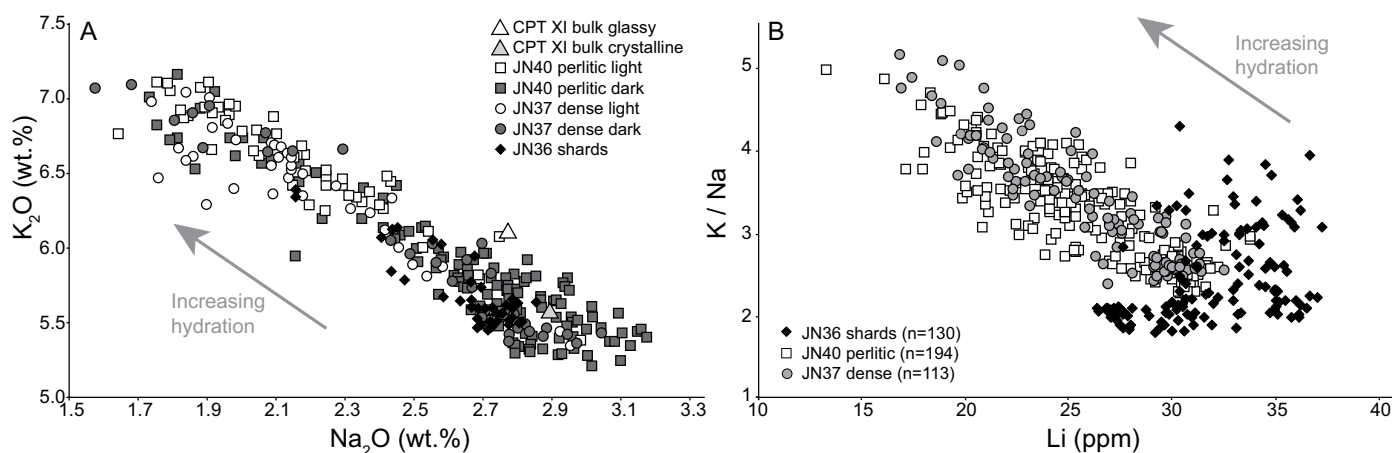


Fig. 3. Compositions of glasses of Cougar Point Tuff XI as a function of glass morphology. A. A subset of the glass compositions (non-normalized) showing K_2O - Na_2O variations as determined by electron probe microanalysis (EPMA). Only shown are glass compositions that are directly linked to a recorded backscatter brightness, as illustrated by the fill of the symbol with those appearing brighter in backscattered electron (BSE imaging) filled white, while those appearing darker filled gray. Also shown are the average bulk rock values of glassy and microcrystalline lithologies of Cougar Point Tuff XI (Bonnichsen et al., 2008), illustrating the general effect of hydration. B. K/Na and Li analyzed using laser ablation-inductively coupled plasma-mass spectrometry. Both panels illustrate the direction of hydration-related compositional changes toward increased K and K/Na and decreased Na and Li .

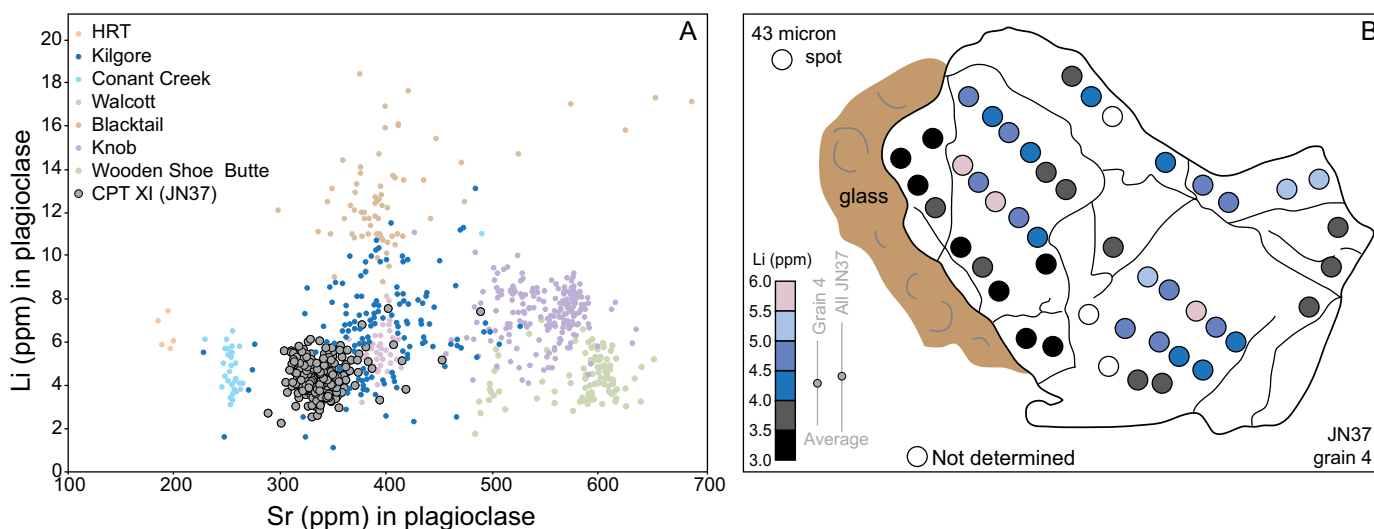


Fig. 4. Lithium distribution in plagioclase. A. Li and Sr contents of plagioclase crystals from vitrophyric samples of Yellowstone-Snake River Plain rhyolites showing little variability in individual units. B. Detail of a single plagioclase crystal from sample JN37 showing Li concentrations between 3.0 and 5.8 ppm. Crystals were selected to have adhering glass to ensure "true" rims were analyzed. Also shown are the average Li content of the single crystal and the population of plagioclase crystals as a whole from JN37.

litic deposits (both ignimbrites and lavas) from the Snake River Plain (Fig. 5). Indeed, this interaction has long been observed in both the products of effusive and explosive Yellowstone-Snake River Plain volcanism (Perkins et al., 1995; Loewen and Bindeman, 2015; Bindeman and Lowenstern, 2016).

The glasses of Cougar Point Tuff XI also preserve evidence of this interaction (Fig. 3). Analytical totals of microprobe measurements average 96.7 wt % (the water by difference method), while the directly measured water contents of the glasses (Table 1) exceed water abundances in pristine volcanic glass (typically <0.3 wt % in fresh obsidians; Friedman and Smith, 1958) as limited by low-pressure solubility

relationships (Newman and Lowenstern, 2002; Ryan et al., 2015).

Like most other hot, dry rhyolites of the Yellowstone-Snake River Plain, Cougar Point Tuff XI contains no hydrous mineral phases that can be used to estimate the magmatic δD value. The most similar analogue comes from the Lava Creek Tuff of Yellowstone, where magmatic amphibole has a δD value of -99‰ , reflecting equilibrium melt values of ca. -70‰ (Loewen and Bindeman, 2015). Magmatic degassing lowers δD values (Taylor et al., 1983) toward values similar to those we report (Table 1). However, such degassing necessarily causes a decrease in the water content rather than the elevat-

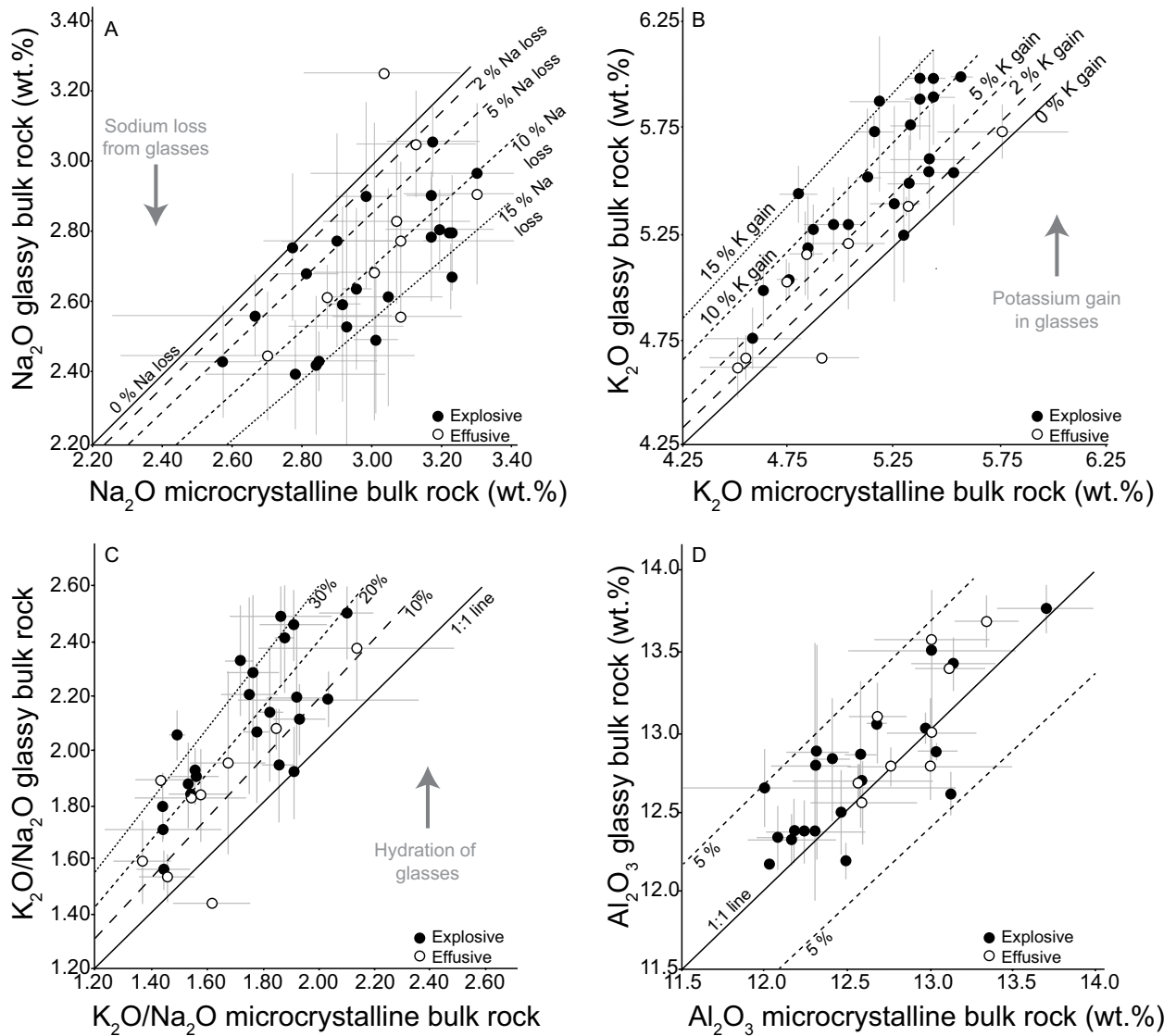


Fig. 5. Diagrams illustrating the effect of hydration as recorded by bulk compositions of both ignimbrites (black) and lavas (white). A single point represents one deposit with the values for both glassy and microcrystalline lithologies reflecting the averages of various amounts of whole rock data. Where shown, the uncertainties represent the standard deviation of results for that lithology for that deposit. Glassy lithologies are distinguished by having lower Na₂O, while both K₂O and K₂O/Na₂O are elevated when compared with their microcrystalline counterparts. Also shown is Al₂O₃ that remains unaffected by the processes of hydration.

ed values found here. Thus, we infer that the δD values of the Cougar Point Tuff XI glass reflect late equilibration with meteoric waters. Using an approximate value of the fractionation factor $\Delta D_{\text{rhyolite-water}}$ estimated by Bindeman and Lowenstern (2016) for the temperatures of formation of Yellowstone perlitites, we can estimate the δD value of the hydration water to be -140 to -118‰ (Table 1). Assuming that the water follows the global average meteoric water line, this corresponds to $\delta^{18}\text{O}_{\text{water}}$ of -19 to -16‰ , both reasonable values for meteoric water at the latitude and altitude of Yellowstone-Snake River Plain where Hildreth et al. (1984) reported modern meteoric water with $\delta^{18}\text{O}$ of -19‰ .

In terms of $\delta^{18}\text{O}$, the rhyolites of the central Snake River Plain represent one of the largest accumulations of low- $\delta^{18}\text{O}$

($<5.5\text{‰}$) magmatic rocks found on Earth (Boroughs et al., 2012). The generation of such low $\delta^{18}\text{O}$ values requires interaction between magma and meteoric water, generally thought to occur by assimilation of previously hydrothermally altered lithologies. In the central Snake River Plain, the ultimate source of the low- $\delta^{18}\text{O}$ magma has been proposed to be the preexisting Idaho batholith (Boroughs et al., 2005), altered caldera lithologies that are down-dropped during multicyclical caldera volcanism (Bindeman et al., 2007), or some combination of these sources (Troch et al., 2020). Regardless of the ultimate source of this signal, the central SRP rhyolites are well characterized to have $\delta^{18}\text{O}$ values between -1.2 and 3.4‰ (Boroughs et al., 2012); Cougar Point Tuff XI has a magmatic $\delta^{18}\text{O}$ value of $\sim -2.8\text{‰}$ determined from measurements

of quartz and plagioclase phenocrysts that indicate high-temperature equilibrium (Boroughs et al., 2012; Bindeman and Simakin, 2014). All the Cougar Point Tuff XI glasses that were measured in this study return $\delta^{18}\text{O}$ values significantly higher than the original magmatic $\delta^{18}\text{O}$ value of 2.8‰, consistent with water-rock interaction at low temperature. Bindeman and Lowenstern (2016) estimated $\Delta^{18}\text{O}_{\text{rhyolite-water}}$ as a function of temperature by combining experimental fractionation factors for albite-water and quartz-water. Using these estimates and assuming a glass fully equilibrated with surrounding meteoric water that follows the meteoric water line, $\delta^{18}\text{O}$ and δD values found in Cougar Point Tuff XI would be indicative of equilibrium at ca. 40° to 70°C. It appears therefore that, at least in the Cougar Point Tuff XI case, glass hydration would have operated in a relatively short time frame following deposition, during the final stages of cooling but distinctly above the ambient temperature.

Behavior of Li with hydration

Based on the data presented in Figures 3 and 5, it is apparent that the glassy portions of the Yellowstone-Snake River Plain rhyolites are being affected by secondary glass hydration and that Li is mimicking the behavior of Na during this process. To ensure that the variability observed in Li is induced by hydration, as opposed to being created by preeruptive magmatic processes, we explored the covariation of Li in a range of units from our sample suite with both K/Na (as an index of hydration; cf. Fig. 3) and trace elements that should be unaffected by hydration to test for magmatic variability (Fig. 6).

Because Li is a moderately incompatible trace element, in a scenario governed only by magmatic processes, Li contents in glass would be expected to correlate positively with incompatible elements such as Rb or Nb and negatively with compatible ones such as Sr. However, such behavior is not observed (Fig. 6), with Li displaying vertical arrays when plotted against Rb and Nb. Li is among the fastest diffusing elements in silicate melt (Holecross et al., 2018), so any potential magmatic variation would be more liable to be erased by diffusion within the melt for Li than other trace elements. Here, where Li varies within any single vitrophyre, we see the opposite, with variations in Li contents but stability in other, slower-diffusing elements. This implies that the variation in Li contents is a post-eruptive process, as supported by the degree of Li variability following the textural appearance of the glass (Fig. 3) and the strong correlation between Li and K/Na. Crystals within the Yellowstone-Snake River Plain rhyolites do not show marked variations in major or trace elements that would be indicative of a strongly changing magmatic system (e.g., Cathey and Nash, 2004; Wolff et al., 2011). From these results, we conclude that during hydration of volcanic glass, Li behaves like Na and may be mobilized from the glass, thus enriching the co-existing water. Textural evidence (Fig. 2) and the stable isotopic compositions of the glasses in Cougar Point Tuff XI suggest that hydration and associated Li loss predominantly occurred at elevated temperatures. Following long (87–97 days) experiments at temperatures between 150° and 350°C at 25 MPa, Cullen et al. (2019) found that a Yellowstone rhyolite starting material lost, on average, 18% of its starting Li content. Other experiments have indicated that Li may also be removed at ambient temperatures. Godfrey et al. (2013) found that a small

proportion (<1.2%) of the Li was removed from volcanic bulk samples of the Cerro Galan and Lascar deposits after 51 days of interaction with distilled water. Such processes may act additionally to provide Li to brine deposits; however, the extent to which these experiments replicate natural settings (e.g., in terms of grain size and surface area) is hard to assess.

How much Li is mobilized with hydration?

To understand the proportion of Li that is lost from the system and so available to form a brine deposit, the starting Li content of the rhyolite is required. Here, we evaluate two potential methods of estimating the original Li content of volcanic glass.

Maximum measured Li content approach: In the maximum measured Li content approach (demonstrated using the data from Cougar Point Tuff XI in Fig. 7), we take the maximum Li content of the glass measured in a sample and use that to define the amount of Li lost in the other measurements. Aside from the maximum measured value, all other measurements provide an estimate of Li loss, the distribution of which can be further described with various statistical parameters. An obvious limitation of this approach is that it relies on the maximum Li content measured from our samples representing the Li content of the groundmass immediately after deposition. In detail, the maximum measured value may be an underestimate, primarily because of the probability of sampling the highest Li value with a necessarily limited number of analyses. The main advantage of this approach is that it may be applied to any glass regardless of specific cooling history.

Mineral-melt partitioning approach: Using partition coefficients, we can invert the Li contents preserved in phenocryst phases (which we can reasonably assume to have been unaffected by hydration as they retain O isotope compositions, reflecting high temperature equilibrium) to estimate Li contents of a melt that would have been in equilibrium with these crystals. Two recent studies (Iveson et al., 2017, 2018) presented Li distribution-coefficient (D) values for plagioclase, clinopyroxene, and amphibole in water-bearing rhyodacitic melts. Here, we use the results of their experiment 1-13-23, which most closely resembles our natural rhyolitic systems (850°C; average melt SiO_2 77.46 ± 0.37 wt % recalculated anhydrous; plagioclase compositions of $\text{An}_{47\pm 2}$) and returns a $D_{\text{Li}^{\text{plag/melt}}}$ value of 0.28 ± 0.2. Because this represents the highest $D_{\text{Li}^{\text{plag/melt}}}$ value of the suite of experiments reported by Iveson et al. (2018), we also use their average $D_{\text{Li}^{\text{plag/melt}}}$ value of 0.23 ± 0.2. However, if the aim is to reconstruct the Li content of the glass following eruptive degassing, then samples must be selected with care (Fig. 8). Where explosive deposits are quenched upon eruption, typically forming nonwelded pumice clasts, plagioclase crystals may exhibit a zonation of Li contents (up to a factor of 4 or so in the case of the Mesa Falls Tuff), with higher Li abundances in crystal cores and lower values at crystal rims and associated with cracks within the crystals (Neukampf et al., 2021). These different domains of Li content within the crystals are reflected in the complex shape of the probability density plot in Figure 8, with a pronounced tail toward lower Li contents reflecting the rims. By contrast, plagioclase crystals in the slowly cooled interiors of deposits have elevated Li contents as a result of groundmass crystallization causing late diffusion from the crystallizing melt into the phenocrysts (Ellis et al., 2018). These crystals

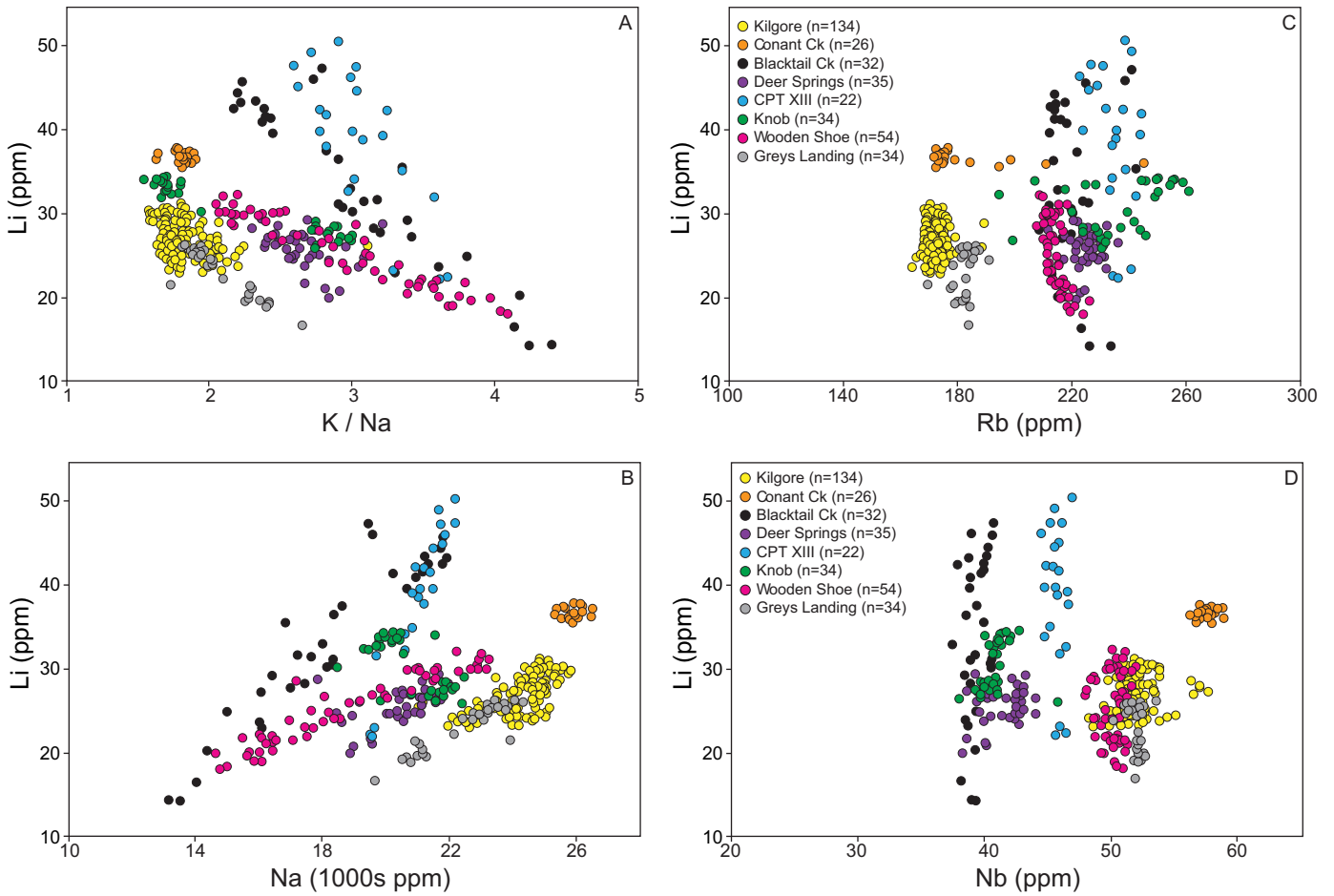


Fig. 6. Variability in Li with components considered mobile and immobile during hydration of selected Yellowstone-Snake River Plain glasses. A and B. Behavior consistent with Li following Na during hydration. C and D. Trace elements that are immobile during hydration are invariant, illustrating that the variability in Li is not a result of a magmatic process.

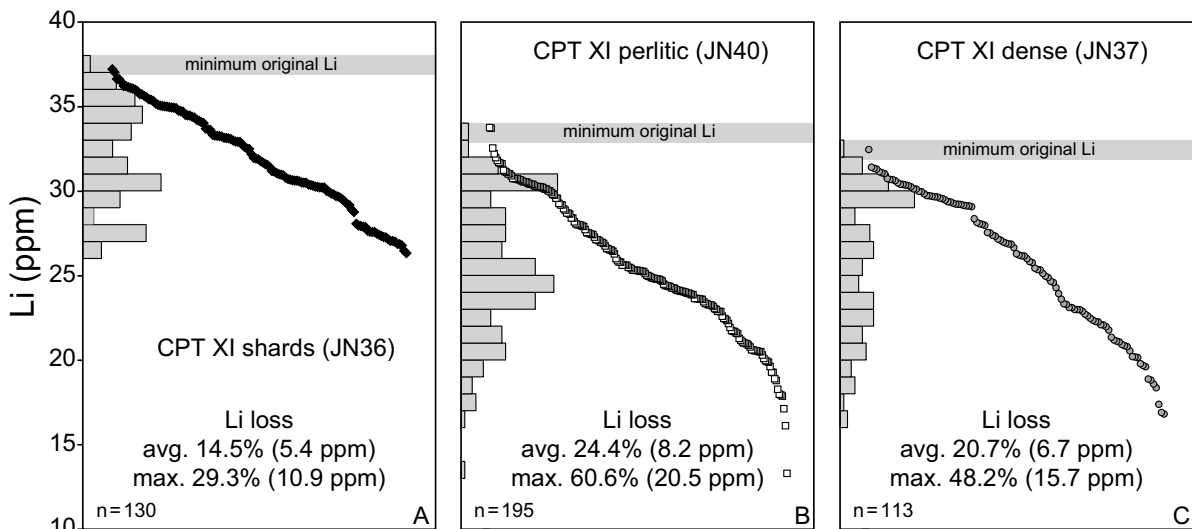


Fig. 7. Illustration of the highest-Li method for estimating Li loss from glassy samples using the three glass morphologies from Cougar Point Tuff XI. Li concentration values representing individual laser ablation-inductively coupled-plasma mass spectrometry spot analyses are rank ordered from highest to lowest in a sample; the difference from the highest Li value ("minimum original Li") to every data point is used as a measure of Li loss. Symbols follow earlier figures.

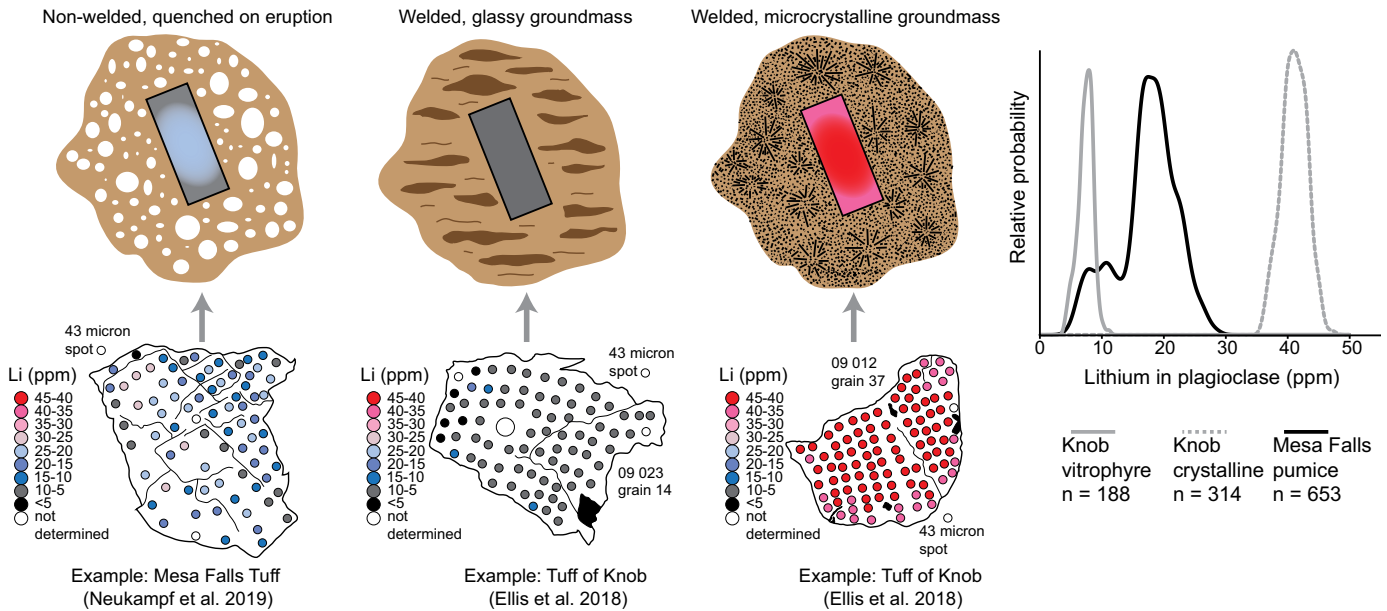


Fig. 8. Schematic of typical distributions of Li in plagioclase crystals from explosive eruptions as a function of variable cooling histories (see Fig. 1). Examples of measured crystals are shown below, and the data from many crystals of the samples illustrated are shown to the right as a probability density plot. This diagram schematically shows why homogeneous crystals from vitrophyres provide the most reliable results for the partitioning approach.

commonly exhibit slightly higher contents of Li in their cores than their rims, indicating Li leaving the crystal after the original enrichment. Finally, plagioclase crystals from dense vitrophyres have Li contents that are homogeneous, having fully equilibrated with the melt following eruptive degassing. These crystals are suitable for the partition-coefficient approach to address Li loss following emplacement.

Use of the highest Li contents of plagioclase crystals may be problematic if the crystals are zoned in Li and have not equilibrated with lower Li contents of the groundmass following degassing (Fig. 8). Thus, Li contents of melt predicted from plagioclase core compositions may provide an overestimate of the starting Li content and thus overestimate the loss of Li post-eruption. This is particularly clear in the case of the Mesa Falls Tuff (Fig. 9) whereby the predicted Li contents of the melts using the Li contents of plagioclase cores are a factor of 2 greater than the highest measured glass value. Based on this, we prefer to use the first approach to estimate the loss of Li. However, as illustrated in Figure 9, the partitioning values are useful in revealing that we are unlikely to be significantly (orders of magnitude) in error when using the highest measured Li content approach.

Lithium loss as a function of time

Taking the regional dataset as a whole, the maximum measured Li content approach returns a Yellowstone-Snake River Plain mean loss of Li of ~22% or 8.9 ppm, with average Li losses among glasses from individual deposits varying between 3 and 57%. Maximum Li losses range from 6 to 85% (Fig. 10). Based on our data, no strong relationship exists between the age of the deposit (so the amount of time available for hydration) and the loss of Li. In line with the timing suggested by the stable isotope values in Cougar Point Tuff XI, glass hydration appears to occur early in the post-eruptive history of the deposits.

An interesting additional point is that from Cougar Point Tuff XI, where the morphology of the glasses provides strong controls on their respective cooling histories, the nonwelded shards have undergone the least Li loss (Fig. 7). This implies that the extent of hydration is controlled by the specific time-temperature history of an individual sample, and samples from vitrophyres, which even while quenching to form glass remain hot longer than fallout shards, are more prone to lose Li. This is supported by the stable isotopic compositions of the glasses that indicate that isotopic exchange between water and glass continued down to temperatures between ~40° and 70°C. The relatively slower cooling vitrophyre samples, as opposed to the rapidly quenched shards, remain longer in this time-temperature window; thus, the loss of Li from these lithologies is more pronounced.

Microcrystalline lithologies

The foregoing discussion centers on the behavior of volcanic glass during post-eruptive hydration, but as noted, the dominant lithology in the Yellowstone-Snake River Plain rhyolites is microcrystalline. The behavior of Li in such lithologies is much less constrained than in volcanic glass, mostly due to the difficulty in measuring Li in materials with such a heterogeneous matrix. Preliminary data from one Snake River Plain ignimbrite (the Tuff of Knob) showed a decrease from ~20 ppm Li in the glassy rock to ~15 ppm in the microcrystalline bulk rock, which was accompanied by a marked shift in $\delta^7\text{Li}$ from ~7.6 to ~14.4‰. This was interpreted as degassing occurring during slow post-eruptive cooling of the deposit (Ellis et al., 2018). Degassing of deposits post-eruption is clear from vesiculated portions of the Yellowstone-Snake River Plain ignimbrites (e.g., Branney et al., 2008; Andrews and Branney, 2011) and at Volcán Chaitén, Lowenstern et al. (2012) suggested that Li (along with other potentially volatile elements)

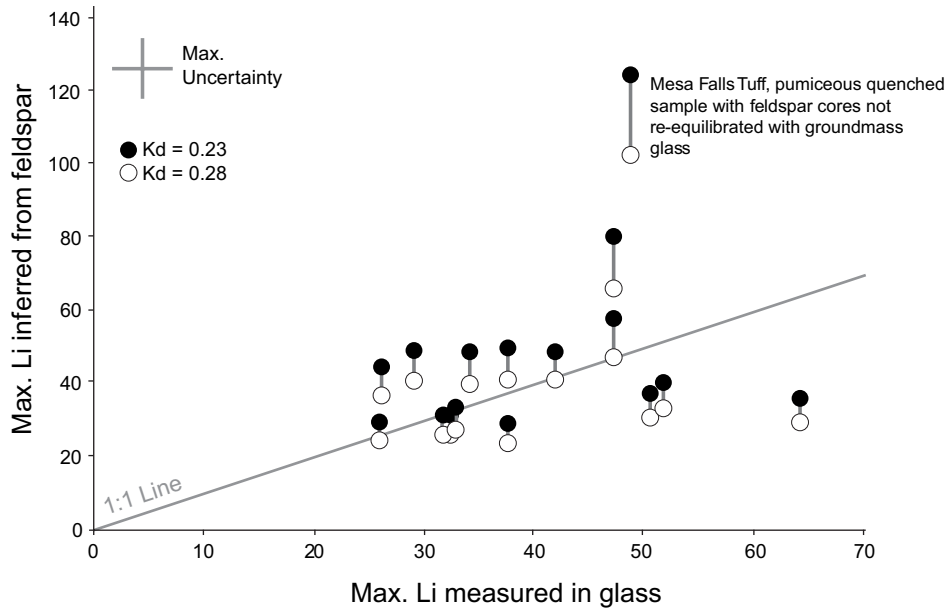


Fig. 9. Comparison of the two methods for estimating the original Li content in the melt at the time of deposition. Overall, the values determined from plagioclase–melt partitioning are in good agreement with the maximum measured Li method. The Mesa Falls Tuff represents an outlier due to that sample being from quenched pumice and the plagioclase crystals retaining diffusion profiles related to magmatic degassing (Neukampf et al., 2019, 2021), schematically shown in Figure 8.

was readily degassed. Thus, there is the potential that post-eruption, the deposit as a whole loses Li, but the mechanism by which the loss occurs is controlled by the cooling history and subsequent lithology of the deposit. If the slowly cooled deposits are degassing Li, then this Li could be dissolved into rainwater, adding further to the available budget.

Estimates of Li available from volcanic glass

With the caveat that loss of Li from microcrystalline lithologies may represent a significant, if underconstrained, contribution to the budget of Li in the hydrologic system, we can use our estimates of the efficiency of hydration of volcanic

glass to produce minimum estimates of the extent to which surficial volcanic rocks could be the source of Li in brine deposits. To do this requires some understanding of the volume of volcanic glass present. The rhyolites of the Yellowstone-Snake River Plain are typically 5 to 10% glassy (by volume), with the majority being microcrystalline flow interiors, and typically having low phenocryst contents (also 5–10%). By taking Li loss values that approximate our average and maximum Li losses, we can then estimate the mass of Li released during hydration of each of the studied deposits (Table 2). To evaluate the variability of other parameters in the Li budget, we also illustrate the effect of the volcanic deposits having 20%

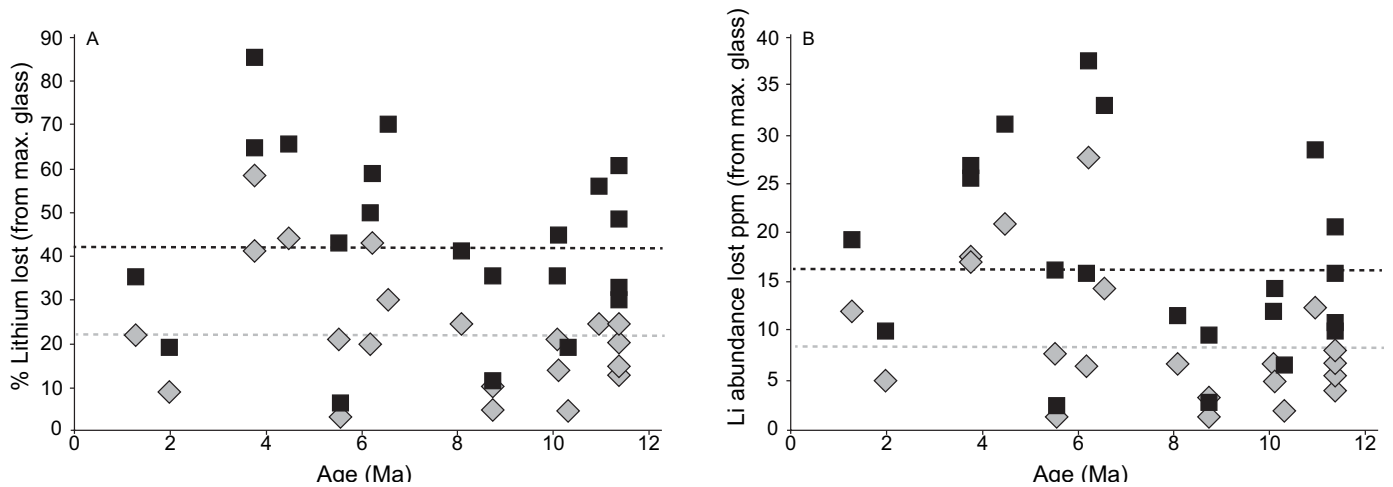


Fig. 10. Chronology of Li loss from the Yellowstone-Snake River Plain deposits using the maximum measured Li methodology. A. Estimated loss of Li from deposits displayed as a percentage, with black reflecting the maximum and gray the average Li loss calculated for each unit as in Figure 7. B. Same results displayed as loss of Li in ppm. Dotted lines show the averages for the maximum and average loss across the two diagrams.

glassy lithologies and having 40% phenocrysts (Fig. 11). This simple analysis reveals that it is very possible to source most of the world's largest documented Li brine deposits entirely by liberating Li from volcanic glass, even if glassy varieties are minor (e.g., 5% of total volume) components of the available rhyolites. For example, 0.2 Mt Li documented in the Rincon deposit in Argentina requires a volume of rhyolite comparable to that of the Mesa Falls Tuff (Table 2). Generating the entire currently documented resource of the Salar de Atacama (6.3 Mt Li; [Bowell et al., 2020](#)) would require the glassy components of >4,000 km³ of high-crystallinity rhyolite losing 20 ppm Li, which is plausible considering the size of the Salar de Atacama catchment and the largely volcanic makeup of the exposed rocks.

The approach we are applying to the availability of Li to make brine deposits is very much centered on the behavior of volcanic glass. We highlight here that it does not take into account the potential water-rock interactions and precipitation of other, potentially Li-hosting minerals occurring between the volcanic deposits and the potential salar. The detailed studies of [Corenthal et al. \(2016\)](#) and [Munk et al. \(2018\)](#) in the Salar de Atacama system illustrate that there may be significant variability in the solute flux into a salar system across the catchment as a whole. [Munk et al. \(2018\)](#) estimate ele-

mental accumulation timescales of different components that range from 0.5 Ma for Mg to 53 Ma for Cl, suggesting that solute sources may change over time or that sources in addition to those measured in present-day waters are required. Such temporal changes would be consistent with the model presented here for the hydration of glass primarily occurring during cooling of the glass shortly after eruption. While our approach does not consider the specific hydrology of a particular salar system, it does place first-order constraints on the behavior of volcanic glass and its suitability as a potential source of Li.

Additional sources of Li to brine deposits

The coherent behavior of Li with other indices of hydration in volcanic glass indicates that it can be mobilized from glass post-eruption. Our estimates from the Yellowstone-Snake River Plain rhyolites indicate that the average of the maximum percentage lost is 43%, with estimates from plagioclase-melt partitioning reinforcing our assumption that the starting Li contents of the glass are reasonable. However, hydration is unlikely to remain the sole source of Li to brine deposits, with contributions likely from degassing of deposits on the surface and magmatic brines. Currently, there remains little agreement on whether Li partitions in favor of

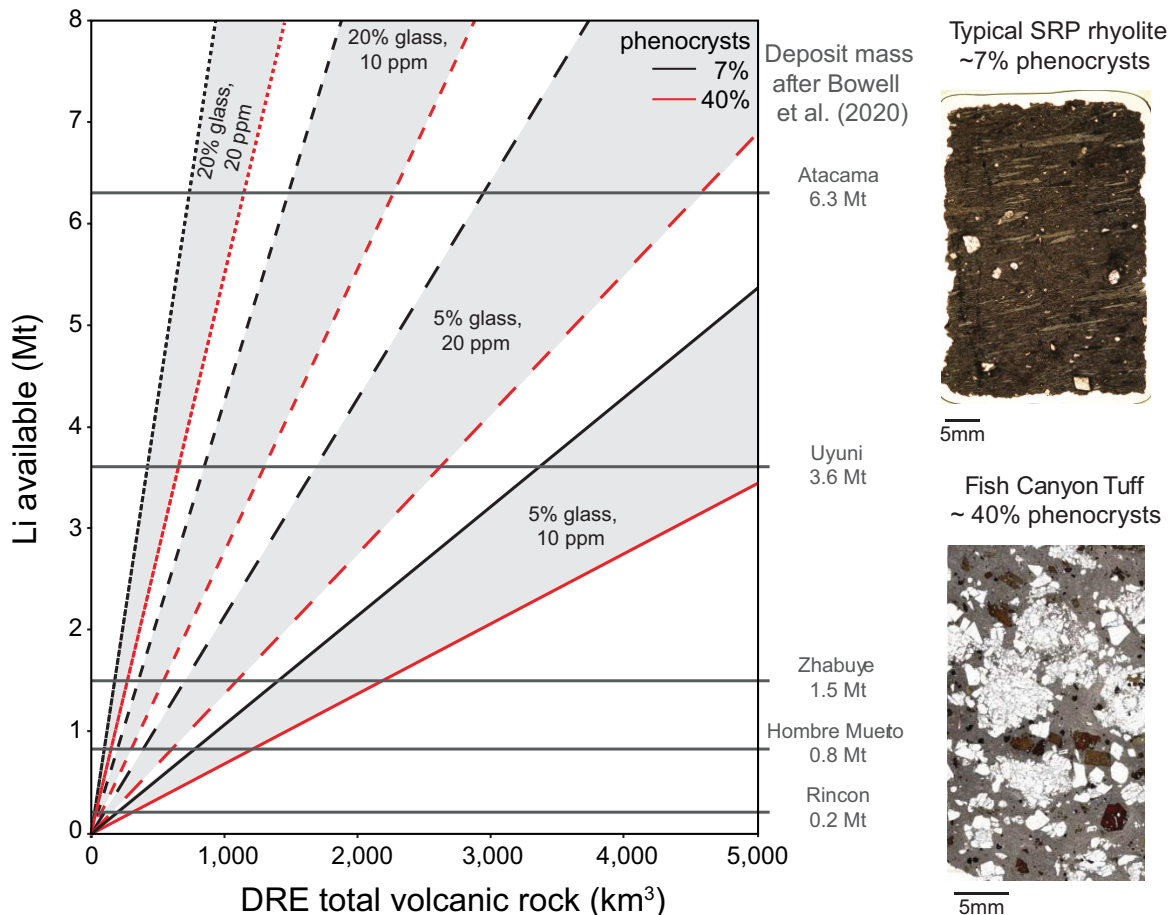


Fig. 11. Diagram illustrating the amount of Li that can be mobilized from volcanic deposits via glass hydration as a function of the proportion of glass in the deposit, the phenocryst content, and the efficiency of the hydration process. For reference, the sizes of several documented Li brine deposits ([Bowell et al., 2020](#)) are shown. DRE = dense rock equivalent, SRP = Snake River Plain.

Table 2. Compilation of Li Data for Units from the Yellowstone-Snake River Plain Province with the Estimated Mass of Li Released for Each Solely from Hydration

Eruptive unit	Location	Age (Ma)	Volume DRE (km ³)	Fraction glassy (%)	Fraction groundmass (%)	Glass mass available (Mt)	Li lost (ppm)		Li lost (Mt)	
							Average	Maximum	Average	Maximum
Mesa Falls Tuff	Yellowstone	1.3	250	5	80	23,000	11.7	19.1	0.27	0.44
Huckleberry Ridge Tuff	Yellowstone	2	2,200	5	85	215,050	4.9	9.8	1.05	2.11
Upper Rhyolite	Heise	3.8	30	5	94	3,243	17.3	27	0.06	0.09
Middle Rhyolite	Heise	3.8	10	5	85	978	17	25.5	0.02	0.02
Kilgore Tuff	Heise	4.48	1,800	5	95	196,650	20.8	30.9	4.09	6.08
Conant Creek Tuff	Heise	5.59	300	5	94	32,430	1.2	2.2	0.04	0.07
Wolverine Creek Tuff	Heise	5.59	80	100	98	180,320	7.7	16.1	1.39	2.90
Lidy Hot Springs	Heise	6.2	20	5	80	1,840	6.2	15.7	0.01	0.03
Walcott Tuff	Heise	6.27	750	5	97	83,663	27.4	37.5	2.29	3.14
Blacktail Creek Tuff	Heise	6.6	1,200	5	80	110,400	14.5	33	1.60	3.64
City of Rocks	CSRP	8.1	1,900	5	80	174,800	6.3	11.5	1.10	2.01
Greys Landing ¹	CSRP	8.72	1,400	5	88	141,680	2.8	9.4	0.40	1.33
Gwin Springs ¹	CSRP	8.72	1,400	5	88	141,680	1.2	2.9	0.17	0.41
Thorn Creek	CSRP	10.1	120	5	85	11,730	4.5	12	0.05	0.14
Wooden Shoe Butte	CSRP	10.14	130	5	88	13,081	6.7	14.2	0.09	0.19
Tuff of Knob	CSRP	10.3	75	5	80	6,900	1.6	6.4	0.01	0.04
CPT XIII	CSRP	11.01	1,470	5	90	152,145	11.7	28.4	1.78	4.32
Rhyolite of Deer Springs	CSRP	11.4	40	5	85	3,910	3.8	9.6	0.01	0.04
CPT XI (dense JN37)	CSRP	11.4	350	5	93	37,433	6.7	15.7	0.25	0.59

Glass density is assumed to be 2,300 kg/m³

Abbreviations: CPT = Cougar Point Tuff; CSRP = central Snake River Plain; DRE = dense rock equivalent

¹These two units were correlated by Knott et al. (2020); as our samples are from widely separated locations, we treat them separately and attribute half the total volume to each; values shown in italics are our estimates; references for geochronology and erupted volume are compiled in Appendix 1, Table A1

the melt (e.g., Iveson et al., 2019) or magmatic fluids (e.g., Webster et al., 1989) under shallow crustal conditions. The variability in physical parameters occurring in these processes (e.g., compositions of fluid phases present) means that they can only be addressed experimentally and that constraining these processes will be crucial to understanding the ultimate Li source for brine deposits.

Conclusions

1. The different glass types in Cougar Point Tuff XI allow the processes of hydration to be compared. The rapidly quenched glass shards from the fallout deposit (sample JN36) have a homogeneous appearance and the smallest range of Li contents. The samples from the vitrophyre (JN37 and JN40) are texturally more variable and show greater variation in Li contents. Li follows the well-understood behavior of Na, suggesting that it is similarly mobilized from volcanic glass by hydration. Oxygen and hydrogen isotopes of glass separates and water contents of the volcanic glass demonstrate that the glasses were hydrated post-eruption.
2. Two approaches (the highest-Li approach and the distribution-coefficient approach) allow the post-eruptive loss of Li from the glass to be estimated. In general, these approaches provide good agreement and suggest that in the Yellowstone-Snake River Plain system, an average of 22% of the Li residing in the glass post-eruption is mobilized. We highlight that the partition-coefficient approach is only reliable in samples from vitrophyres where the cooling rate is fast enough to produce a glass but slow enough to allow Li in the crystal to fully equilibrate with the melt on the surface. Plagioclase crystals from immediately quenched samples of tephra may preserve gradients in Li

abundances that result from syneruptive degassing, while crystals in the microcrystalline interiors have Li contents that are significantly elevated during crystallization of the groundmass.

3. Within the Snake River Plain, over approximately 10 m.y. covered in this study, there is no relationship between the estimated loss of Li from a glass sample and the age of the sample. Oxygen and hydrogen isotope compositions of the glasses suggest that the last exchange between water and glass occurred at temperatures slightly but distinctly higher than ambient. This suggests that the hydration of the deposit and potential loss of Li occur during a finite period constrained by the cooling history of that deposit.
4. By combining the Li loss from Yellowstone-Snake River Plain glasses with geologically realistic estimates of phenocryst content and the proportion of deposit that remains glassy, we can make first-order estimates of the total amount of Li lost from volcanic deposits. Liberating 6 Mt of Li (akin to the entire Atacama deposit) would require 3,000 to 4,000 km³ of rhyolite losing 20 ppm Li, but smaller deposits (e.g., Rincon) can be generated from only a few hundred cubic kilometers of rhyolite.

Acknowledgments

We would like to gratefully acknowledge financial support from the Swiss National Science Foundation (grant 200021_166281 to BE). Discussions with Colin Macpherson helped focus our ideas. Juliana Troch provided typically excellent support in the field. We also acknowledge Sherissa Roopnarain for help with O and H analyses. We would also like to thank Dr. Thomas Benson (Lithium Americas) and an anonymous reviewer for their detailed comments that helped improve the manuscript. *Economic Geology* editors Dr. Larry Meinert and Dr.

Paul Spry provided additional helpful input to the paper and showed admirable patience with our sluggish revision.

REFERENCES

- Anderson, A.T., Davis, A.M., and Lu, F., 2000, Evolution of Bishop Tuff rhyolitic magma based on melt and magnetite inclusions and zoned phenocrysts: *Journal of Petrology*, v. 41, p. 449–473.
- Andrews, G.D.M., and Branney, M.J., 2011, Emplacement and rheomorphic deformation of a large, lava-like rhyolitic ignimbrite: Grey's Landing, southern Idaho: *Geological Society of America Bulletin*, v. 123, p. 725–743.
- Benson, T.R., Coble, M.A., Rytuba, J.J., and Mahood, G.A., 2017a, Lithium enrichment in intracontinental rhyolite magmas leads to Li deposits in caldera basins: *Nature Communications*, v. 8, 270.
- Benson, T.R., Mahood, G.A., and Grove, M., 2017b, Geology and $^{40}\text{Ar}/^{39}\text{Ar}$ geochronology of the middle Miocene McDermitt volcanic field, Oregon and Nevada: Silicic volcanism associated with propagating floor basalt dikes at initiation of the Yellowstone hotspot: *Geological Society of America Bulletin*, v. 129, p. 1027–1051.
- Bibienne, T., Magnan, J.F., Rupp, A., and Laroche, N., 2020, From mine to mind and mobiles: Society's increasing dependence on lithium: *Elements*, v. 16, p. 265–270.
- Bindeman, I.N., Watts, K.E., Schmitt, A.K., Morgan, L.A., and Shanks, P.W., 2007, Voluminous low $\delta^{18}\text{O}$ magmas in the late Miocene Heise volcanic field, Idaho: Implications for the fate of Yellowstone hotspot calderas: *Geology*, v. 35, p. 1019–1022.
- Bindeman, I.N., and Lowenstern, J.B., 2016, Low- δD hydration rinds in Yellowstone perlitites record rapid syneruptive hydration during glacial and interglacial conditions: *Contributions to Mineralogy and Petrology*, v. 171, 89.
- Bindeman, I.N., and Simakin, A.G., 2014, Rhyolites—Hard to produce, but easy to recycle and sequester: Integrating microgeochemical observations and numerical models: *Geosphere*, v. 10, 5, p. 930–957.
- Bonnichsen, B., and Citron, G.P., 1982, The Cougar Point Tuff, southwestern Idaho and vicinity, in Bonnichsen, B., and Breckenridge, R.M., eds., *Cenozoic geology of Idaho*: Idaho Bureau of Mines Geology Bulletin 26, p. 255–281.
- Bonnichsen, B., Leeman, W.P., Honjo, N., McIntosh, W.C., and Godchaux, M.M., 2008, Miocene silicic volcanism in southwestern Idaho: Geochronology, geochemistry, and evolution of the central Snake River Plain: *Bulletin of Volcanology*, v. 70, p. 315–342.
- Boroughs, S., Wolff, J., Bonnichsen, B., Godchaux, M., and Larson, P., 2005, Large-volume, low- $\delta^{18}\text{O}$ rhyolites of the central Snake River Plain, Idaho, USA: *Geology*, v. 33, p. 821–824.
- Boroughs, S., Wolff, J.A., Ellis, B.S., Bonnichsen, B., and Larson, P.B., 2012, Evaluation of models for the origin of Miocene low- $\delta^{18}\text{O}$ rhyolites of the Yellowstone/Columbia River Large Igneous Province: *Earth and Planetary Science*, v. 313, p. 45–55.
- Bowell, R.J., Lagos, L., de los Hoyos, C.R., and Declercq, J., 2020, Classification and characteristics of natural lithium resources: *Elements*, v. 16, p. 259–264.
- Bradley, D., Munk, L., Jochens, H., Hynek, S., and Labay, K., 2013, A preliminary deposit model for lithium brines: U.S. Geological Survey Open-File Report 2013-1006, 6 p.
- Branney, M.J., Bonnichsen, B., Andrews, G.D.M., Ellis, B., Barry, T.L., and McCurry, M., 2008, Snake River (SR)-type volcanism at the Yellowstone hotspot track: Distinctive products from unusual, high-temperature silicic super-eruptions: *Bulletin of Volcanology*, v. 70, p. 293–314.
- Castor, S.B., and Henry, C.D., 2020, Lithium-rich claystone in the McDermitt caldera, Nevada, USA: Geologic, mineralogical, and geochemical characteristics and possible origin: *Minerals*, v. 10, 68.
- Cathey, H.E., and Nash, B.P., 2004, The Cougar Point Tuff: Implications for thermochemical zonation and longevity of high-temperature, large-volume silicic magmas of the Miocene Yellowstone hotspot: *Journal of Petrology*, v. 45, p. 27–58.
- Chen, C., Lee, C.-T.A., Tang, M., Biddle, K., and Sun, W., 2020, Lithium systematics in global arc magmas and the importance of crustal thickening for lithium enrichment: *Nature Communications*, v. 11, 5313.
- Corenthal, L.G., Boutt, D.F., Hynek, S.A., and Munk, L.A., 2016, Regional groundwater flow and accumulation of a massive evaporite deposit at the margin of the Chilean Altiplano: *Geophysical Research Letters*, v. 43, p. 8017–8025.
- Cullen, J.T., Hurwitz, S., Barnes, J.D., Lassiter, J.C., Penniston-Dorland, S., Kasemann, S.A., and Thordsen, J.J., 2019, Temperature-dependent variations in mineralogy, major element chemistry and the stable isotopes of boron, lithium and chlorine resulting from hydration of rhyolite: Constraints from hydrothermal experiments at 150 to 350 °C and 25 MPa: *Geochimica Cosmochimica Acta*, v. 261, p. 269–287.
- Donovan, J., Kremser, D., and Fournelle, J., 2007, Probe for Windows user's guide and reference, enterprise edition, Probe software, Inc.: Eugene, OR.
- Dunbar, N.W., and Hervig, R.L., 1992, Petrogenesis and volatile stratigraphy of the Bishop Tuff: Evidence from melt inclusion analysis: *Journal of Geophysical Research*, v. 97, p. 15129–15150.
- Ellis, B.S., Branney, M.J., Barry, T.L., Barford, D., Wolff, J.A., Bonnichsen, B., and Bindeman, I.N., 2012, Three newly discovered super-eruptions from the Yellowstone hotspot track, Idaho, USA: *Bulletin of Volcanology*, v. 75, p. 261–277.
- Ellis, B.S., Cordonnier, B., Rowe, M.C., Szymanowski, D., Bachmann, O., and Andrews, G.D.M., 2015, Groundmass crystallisation and cooling rates of lava-like ignimbrites: the Grey's Landing ignimbrite, southern Idaho, USA: *Bulletin of Volcanology*, v. 77, 87.
- Ellis, B.S., Szymanowski, D., Wotzlaw, J.F., Schmitt, A.K., Bindeman, I.N., Troch, J., Harris, C., Bachmann, O., and Guillong, M., 2017, Post-caldera volcanism at the Heise volcanic field: implications for petrogenetic models: *Journal of Petrology*, v. 58, p. 115–136.
- Ellis, B.S., Szymanowski, D., Magna, T., Neukampf, J., Dohmen, R., Bachmann, O., Ulmer, P., and Guillong, M., 2018, Post-eruptive mobility of lithium in volcanic rocks: *Nature Communications*, v. 9, 3228.
- Friedman, I., and Smith, R.L., 1958, The deuterium content of water in some volcanic glasses: *Geochimica et Cosmochimica Acta*, v. 15, p. 218–228.
- Godfrey, L.V., Chan, L.H., Alonso, R.N., Lowenstein, T.K., McDonough, W.F., Houston, J., Li, J., Bobst, A., and Jordan, T.E., 2013, The role of climate in the accumulation of lithium-rich brine in the Central Andes: *Applied Geochemistry*, v. 38, p. 92–102.
- Guillong, M., Meier, D., Allan, M., Heinrich, C., and Yardley, B., 2008, SILLS: A MATLAB-based program for the reduction of laser ablation ICP-MS data of homogeneous materials and inclusions, in Sylvester, P., ed., *Laser ablation ICP-MS in the earth sciences: Current practices and outstanding issues*: Mineralogical Association of Canada Short Course 40, p. 328–333.
- Harris, C., Compton, J.S., and Bevington, S.A., 1999, Oxygen and hydrogen isotope composition of kaolinite deposits, Cape Peninsula, South Africa: Low-temperature, meteoric origin: *Economic Geology*, v. 94, p. 1353–1366.
- Harris, C., Johnstone, W.P., and Phillips, D., 2002, Petrogenesis of the Mesozoic Sistejell syenite intrusion, Dronning Maud Land, Antarctica and surrounding low- $\delta^{18}\text{O}$ lavas: *South African Journal of Geology*, v. 105, p. 205–226.
- Henry, C.D., Castor, S.B., Starkel, W.A., Ellis, B.S., Wolff, J.A., Laravie, J.A., McIntosh, W.C., and Heizler, M.T., 2017, Geology and evolution of the McDermitt caldera, northern Nevada and southeastern Oregon, western USA: *Geosphere*, v. 13, p.1066–1112.
- Hildreth, W.E., Christiansen, R.L., and O'Neil, J.R., 1984, Catastrophic isotopic modification of rhyolitic magma at times of caldera subsidence, Yellowstone Plateau Volcanic Field: *Journal of Geophysical Research*, v. 89, p. 8339–8369.
- Hofstra, A.H., Todorov, T.I., Mercer, C.N., Adams, D.T., and Marsh, E.E., 2013, Silicate melt inclusion evidence for extreme pre-eruptive enrichment and post-eruptive depletion of lithium in silicic volcanic rocks of the western United States: Implications for the origin of lithium-rich brines: *Economic Geology*, v. 108, p. 1691–1701.
- Holycross, M.E., Watson, E.B., Richter, F.M., and Villeneuve, J., 2018, Diffusive fractionation of Li isotopes in wet, highly silicic melts: *Geochemical Perspectives Letters*, v. 6, p. 39–42.
- Iveson, A.A., Webster, J.D., Rowe, M.C., and Neill, O.K., 2017, Major element and halogen (F, Cl) mineral–melt–fluid partitioning in hydrous rhyodacitic melts at shallow crustal conditions: *Journal of Petrology*, v. 58, p. 2465–2492.
- Iveson, A.A., Rowe, M.C., Webster, J.D., and Neill, O.K., 2018, Amphibole-, clinopyroxene- and plagioclase-melt partitioning of trace and economic metals in halogen-bearing rhyodacitic melts: *Journal of Petrology*, v. 59, p. 1579–1604.
- Iveson, A.A., Webster, J.D., Rowe, M.C., and Neill, O.K., 2019, Fluid–melt trace-element partitioning behaviour between evolved melts and aqueous fluids: Experimental constraints on the magmatic-hydrothermal transport of metals: *Chemical Geology*, v. 516, p. 18–41.

- Jezeck, P.A., and Noble, D.C., 1978, Natural hydration and ion exchange of obsidian: An electron microprobe study: *American Mineralogist*, v. 63, p. 266–273.
- Jochum, K.P., Nohl, U., Herwig, K., Lammel, E., Stoll, B., and Hofmann, A.W., 2005, GeoReM: A new geochemical database for reference materials and isotopic standards: *Geostandards and Geoanalytical Research*, v. 29, p. 333–338.
- Kent, A.J.R., Blundy, J., Cashman, K.V., Cooper, K.M., Donnelly, C., Pallister, J.S., Reagan, M., Rowe, M.C., Thornber, C.R., 2007, Vapor transfer prior to the October 2004 eruption of Mount St. Helens, Washington: *Geology*, v. 35, p. 231–234.
- Kesler, S.E., Gruber, P.W., Medina, P.A., Keolian, G.A., Everson, M.P., and Wallington, T.J., 2012, Global lithium resources: Relative importance of pegmatite, brine and other deposits: *Ore Geology Reviews*, v. 48, p. 55–69.
- Knott, T.R., Branney, M.J., Reichow, M.K., Finn, D.R., Tapster, S., and Coe, R.S., 2020, Discovery of two new super-eruptions from the Yellowstone hotspot track (USA): Is the Yellowstone hotspot waning? *Geology*, v. 48, p. 934–938.
- Lipman, P.W., 1965, Chemical comparison of glassy and crystalline volcanic rocks: U.S. Geological Survey Bulletin 1201-D, p. 1–24.
- Lipman, P.W., Christiansen, R.L., and van Alstine, E.A., 1969, Retention of alkalis by calc-alkalic rhyolite during crystallization and hydration: *American Mineralogist*, v. 54, p. 285–291.
- Loewen, M.W., and Bindeman, I.N., 2015, Oxygen isotope and trace element evidence for three-stage petrogenesis of the youngest episode (260–79 ka) of Yellowstone rhyolitic volcanism: *Contributions to Mineralogy and Petrology*, v. 170, 39.
- London, D., and Morgan, G.B., 2017, Experimental crystallization of the Macusani obsidian, with applications to lithium-rich granitic pegmatites: *Journal of Petrology*, v. 58, p. 1005–1030.
- Lowenstein, T.K., and Risacher, F., 2009, Closed basin brine evolution and the influence of Ca–Cl inflow waters: Death Valley and Bristol Dry Lake California, Qaidam Basin, China, and Salar de Atacama, Chile: *Aquatic Geochemistry*, v. 15, p. 71–94.
- Lowenstein, J.B., Bleick, H., Vazquez, J.A., Castro, J.M., and Larson, P.B., 2012, Degassing of Cl, F, Li, and Be during extrusion and crystallization of the rhyolite dome at Volcán Chaitén, Chile during 2008 and 2009: *Bulletin of Volcanology*, v. 74, p. 2303–2319.
- Munk, L.A., Hynek, S.A., Bradley, D.C., Boutt, D., Labay, K., and Jochens, H., 2016, Lithium brines: A global perspective: *Reviews in Economic Geology*, v. 18, p. 339–365.
- Munk, L.A., Boutt, D.F., Hynek, S.A., and Moran, S.J., 2018, Hydrogeochemical fluxes and processes contributing to the formation of lithium-enriched brines in a hyper-arid continental basin: *Chemical Geology*, v. 493, p. 37–57.
- Myers, M.L., Wallace, P.J., Wilson, C.J.N., Morter, B.M., and Swallow, E.J., 2016, Prolonged ascent and episodic venting of discrete magma batches at the onset of the Huckleberry Ridge supereruption, Yellowstone: *Earth and Planetary Science Letters*, v. 451, p. 285–297.
- Neukampf, J., Ellis, B.S., Magna, T., Laurent, O., and Bachmann O., 2019, Partitioning and isotopic fractionation of lithium in mineral phases of hot, dry rhyolites: The case of the Mesa Falls Tuff, Yellowstone: *Chemical Geology*, v. 506, p. 175–186.
- Neukampf, J., Ellis, B.S., Laurent, O., Steinmann, L.K., Ubide, T., Oeser, M., Magna, T., Weyer, S., and Bachmann, O., 2021, Time scales of syn-eruptive volatile loss in silicic magmas quantified by Li-isotopes: *Geology*, v. 49 (2), p. 125–129.
- Newman, S., and Lowenstein, J.B., 2002, VolatileCalc: A silicate melt–H₂O–CO₂ solution model written in Visual Basic for Excel: *Computers & Geosciences*, v. 28, p. 597–604.
- Noble, D.C., 1967, Sodium, potassium and ferrous iron contents of some secondarily hydrated natural silicic glasses. *American Mineralogist*, v. 52, p. 280–286.
- Perkins, M.E., Nash, W.P., Brown, F.H., and Fleck, R.J., 1995, Fallout tuffs of Trapper Creek Idaho—a record of Miocene explosive volcanism in the Snake River Plain volcanic province: *Geological Society of America Bulletin*, v. 107, p. 1484–1506.
- Ryan, A.G., Russell, J.K., Nichols, A.R., Hess, K.U., and Porritt, L.A., 2015, Experiments and models on H₂O retrograde solubility in volcanic systems: *American Mineralogist*, v. 100, p. 774–786.
- Sterba, J., Krzemien, A., Fernandez, P.R., Garcia-Miranda, C.E., and Valverde, G.F., 2019, Lithium mining: Accelerating the transition to sustainable energy: *Resources Policy*, v. 62, p. 416–426.
- Stix, J., and Layne, G.D., 1996, Gas saturation and evolution of volatile and light lithophile elements in the Bandelier magma chamber between two caldera-forming eruptions: *Journal of Geophysical Research*, v. 101, p. 25181–25196.
- Swallow, E.J., Wilson, C.J.N., Charlier, B.L.A., and Gamble, J.A., 2019, The Huckleberry Ridge Tuff, Yellowstone: Evacuation of multiple magmatic systems in a complex episodic eruption: *Journal of Petrology*, v. 60, p. 1371–1426.
- Szymanowski, D., Ellis, B.S., Bachmann, O., Guillon, M., and Phillips, W.M., 2015, Bridging basalts and rhyolites in the Yellowstone-Snake River Plain volcanic province: The elusive intermediate step: *Earth and Planetary Science Letters*, v. 415, p. 80–89.
- Taylor, B.E., Eichelberger, J.C., and Westrich, H.R., 1983, Hydrogen isotopic evidence of magma degassing during shallow intrusion and eruption: *Nature*, v. 306, p. 541–545.
- Tomascak, P.B., Magna, T., and Dohmen, R., 2016, *Advances in lithium isotope geochemistry*: Cham, Springer, 195 p.
- Troch, J., Ellis, B.S., Harris, C., Bachmann, O., and Bindeman, I.N., 2020, Low- $\delta^{18}\text{O}$ silicic magmas on Earth: A review: *Earth Science Reviews*, v. 208, 103299.
- Vennemann, T.W., and O'Neil, J.R., 1993, A simple and inexpensive method of hydrogen isotope and water analysis of minerals and rocks based on zinc reagent: *Chemical Geology*, v. 103, p. 227–234.
- Vennemann, T.W., and Smith, H.S., 1990, The rate and temperature of reaction of CIF₃ with silicate minerals, and their relevance to oxygen isotope analysis: *Chemical Geology*, v. 86, p. 83–88.
- Wallace, P.J., Anderson, A.T., and Davis, A.M., 1999, Gradients in H₂O, CO₂, and exsolved gas in a large-volume silicic magma system: Interpreting the record preserved in melt inclusions from the Bishop Tuff: *Journal of Geophysical Research*, v. 104, p. 20097–20122.
- Webster, J.D., Holloway, J.R., and Hervig, R.L., 1989, Partitioning of lithophile trace elements between H₂O and H₂O + CO₂ fluids and topaz rhyolite melt: *Economic Geology*, v. 84, p. 116–134.
- Wolff, J.A., Ellis, B.S., and Ramos, F.C., 2011, Strontium isotopes and magma dynamics: Insights from high-temperature rhyolites: *Geology*, v. 39, p. 931–934.



Ben Ellis is a volcanologist with more than 15 years of experience working on evolved magmas in a variety of geologic settings. He is particularly interested in the behavior of lithium (Li) in shallow silicic magmatic systems in terms of how Li may be removed from silicate melt via degassing or fluid exsolution. To address these issues, Ben and a range of collaborators combine field-based measurements with experimental studies. Ben holds a Ph.D. from the University of Leicester (U.K.) and is currently a senior scientist in the Magmatic Petrology group at ETH Zürich.

